Analyzing HDPE geomembrane wrinkle overlying sand subgrade using a finite-discrete element framework

Masood Meidani [1], Mohamed A. Meguid [2] & Luc E. Chouinard [2]
(1) Graduate student, (2) Associate Professor
Department of Civil engineering and applied mechanics, McGill University
Montreal. QC, Canada, H3A 0C3

ABSTRACT
High-density polyethylene (HDPE) geomembranes (GM) are commonly used as barrier systems in solid waste landfills as they provide a relatively low hydraulic conductivity. Wrinkles are formed in geomembrane during installation as a result of material expansion due to solar heating or placement of backfill materials. In this research, a coupled finite-discrete element model has been developed to examine the behavior of geomembrane wrinkle placed between firm sand subgrade and gravelly drainage layer. The geomembrane is modeled using finite elements (FE) whereas the drainage layer and the foundation soil are modeled using discrete elements (DE). To transfer the contact forces and displacements between the DE and FE domains, triangular shaped facet interface elements are adopted. The analysis is performed based on an experimental configuration reported in the literature. The effects of the subgrade properties, backfill material and overburden pressure on the wrinkle deformation are investigated. Results show that the presence of wrinkle increases the local strains in the geomembrane right next to the deformed wrinkle. Applying vertical pressure of up to 1100 kPa resulted only in a slight reduction in the size of the gap beneath the geomembrane. Among the different factors, the wrinkle deformation is significantly influenced by the change in subgrade properties and the applied pressure. The numerical results proved the efficiency of the coupled framework in modeling GM-soil interactions problems.

RÉSUMÉ
Les géomembranes en polyéthylène haute densité (PEHD) sont couramment utilisées comme systèmes de barrières dans les sites d'enfouissement des déchets solides car elles fournissent une conductivité hydraulique relativement faible. Des plis sont formées dans la géomembrane pendant le processus d'installation en raison de l'expansion du matériau par chauffage solaire ou lors du placement de matériaux de remblai. Dans cette recherche, un modèle par éléments finis couplé à un modèle par éléments discret a été développé pour examiner le comportement des plis pour une géomembrane insérée entre une couche de sable ferme et une couche de gravier drainant. La géomembrane est modélisée à l'aide des éléments finis (FE) tandis que la couche de gravier drainant et la fondation sont modélisées à l'aide d'éléments discrets (DE). Les forces de contact et les déplacements entre les domaines discrets (DE) et continus (FE) sont modélisés avec des éléments d'interface triangulaires. Le modèle est uilisé pour reproduire les conditions et les résultats expérimenaux d'un essai rapporté dans la littérature. L'influence des propriétés de la sous-couche de fondation, du matériau de remblai et de la surcharge sur la géométrie des plis sont étudiés. Les résultats montrent que la présence des plis augmente les déformations relatives à proximité des plis. L'application d'une pression de 1100 kPa réduit faiblement le volume de a cavité sous le pli. Parmi les divers facteurs étudiés, les propriétés de la couche de fondation et la pression appliquée ont le plus d'influence sur la déformation des plis. Les résultats numériques démontrent l'efficacité de la modélisation couplée (FE-DE) pour analyser le couplage entre le sol et les géomembranes.

1 INTRODUCTION

High-density polyethylene geomembrane has been widely used in municipal solid waste landfills as a hydraulic barrier system due to the low permeability and ease of installation. Development of holes in the geomembrane can be considered as one of the greatest risks in landfill serviceability. Damage during GM installation; puncture due to placement of overlying drainage layer, and stress-cracking that results from the long-term tensile strains are major factors that lead to the development of holes (Rowe et al., 2004).

Wrinkles in the geomembrane can extend the damage as the gap under the wrinkle prevents contacts between the GM and the underlying material. Redistribution of vertical stresses under the wrinkles induces tensile strains on both sides of the wrinkle. These strains can be compounded by other tensile strains from indentation caused by the drainage layer, and increase the potential for stress-related cracking. Wrinkles can also develop in the GM due to the material expansion caused by solar heating or the placement of the overlying drainage layer.

Deformations and strains developing in the wrinkle are functions of the material types below and above the GM. Soong and Koerner (1998) performed a series of experiments to measure the wrinkle deformations for the cases wherethe GM is placed between two sand layers. The study showed that the height and width of the wrinkle are reduced, but the gap beneath the wrinkle remained. Gudina and Brachman (2006) reported the short-term response of GM wrinkles overlying compacted clays at two different initial water contents. Results showed that the gap was eliminated depending on the vertical pressure and the water content of the clay. Furthermore, Brachman and Gudina (2008) investigated GM strains caused by indentation of coarse gravel and wrinkles in a

GM/GCL composite liner. Wrinkle height and width decreased in all tests, however the gap remained beneath the GM/GCL liner when a firm sand layer was placed as a foundation.

The objective of this research is to present a coupled finite-discrete element framework which is used to evaluate the response of the HDPE geomembrane wrinkles overlying sand subgrade. The numerical model is developed based on the experiments published by Brachman and Gudina (2008). The geomembrane layer is placed between sand foundation and coarse gravel drainage layer. Finite elements (FE) approach is used to model the geomembrane, while the soil domain is created using discrete elements (DE). A brief explanation of the experiments is presented followed by a short description of the numerical framework used in the analysis. Emphasis is placed in this study on the effects of the sand and gravel properties on the wrinkle deformation and geometry. Also, the effect of the overburden pressure on the wrinkle response is evaluated.

2 EXPERIMENTAL STUDY

The general configuration of the numerical simulation was based on the experimental study by Brachman and Gudina (2008). A cylindrical steel pressure vessel with an inside diameter of 590 mm and a height of 500 mm was used in the experiments. The sample includes 150 mm foundation layer overlain by GM with or without geotextile (GT) sheet as a protection covered with 300 mm coarse gravel and 50 mm of leveling sand. After placing the materials, a vertical pressure is applied in increments. The sample is maintained under the applied pressure for 10 hours. Then a low-shrinkage grout is injected into the GM to maintain the geometry of the gap and the GM. Afterward, pressure is released and the drainage layer is removed. The final deformation, height and width of the wrinkle are measured.

Table 1. Material properties of HDPE geomembrane

Properties	Value
Thickness (mm)	1.5
Density (g/cc)	0.94
Tensile strength at yield (kN/m)	31
Tensile elongation at yield (%)	18
2% secant modulus (MPa)	300

The foundation layer beneath the GM was dry poorly graded medium-sand (SP). The sand was compacted to reach a density index of 85% corresponding to a dry density of 1.91 g/cm^3. The drainage layer overlying the GM was poorly graded coarse gravel (GP) as per the requirements of Ontario, Canada landfill regulations (MOE, 1998). This layer was placed in a loose condition with a dry density of 1.72 g/cm^3. Grain size distribution curves of these two layers are presented in Fig. 1.

The properties of the GM are presented in Table 1. A wrinkle is manually formed in the GM with an initial height of 60 mm and width of 240 mm. The used wrinkle geometry is consistent with Pelte et al. (1994) field observations.

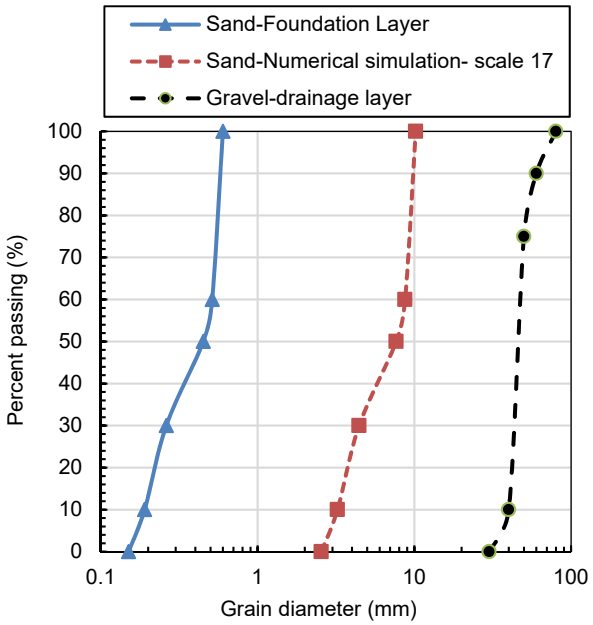

Figure 1. Particle size distribution of the drainage layer and sand subgrade in the experiment and numerical simulation

3 COUPLED FINITE-DISCRETE ELEMENT FRAMEWORK

The coupled FE-DE framework is a continuation of the work of Dang and Meguid (2010a, 2013). YADE (Kozicki and donze, 2009; Smilauer et al., 2010) open source discrete element code is used as a platform to develop the coupled framework. The algorithm of the coupled numerical simulation is briefly described below.

3.1 Finite elements

A dynamic relaxation approach is used in the coupled framework to solve the equations of the FE domain. The general equation that needs to be solved is:

$$K\,\boldsymbol{X} + cM\dot{\boldsymbol{X}} + M\,\ddot{\boldsymbol{X}} = \boldsymbol{P} \quad (1)$$

Where, K is the stiffness matrix, c is the damping coefficient for the mass proportional damping, M is the mass matrix, P is the external force vector and $\boldsymbol{X}$ represents the displacement vector.

In order to satisfy the convergence condition, time step $[\Delta t_{FE}]$ is determined using the maximum eigenvalue:

$$\Delta t_{FE} \leq [\Delta t_{FE}] = \frac{2}{\sqrt{\lambda_m}} \quad (2)$$

where, λ_m is the maximum eigenvalue,

$$\lambda_m \leq \max_i \sum_{j=1}^{n} \frac{k_{ij}}{M_{ij}} \quad (3)$$

3.2 Discrete elements

The interaction between particles is simulated using a contact model that considers traction, compression, bending and twisting with cohesion and friction based on

Mohr-Coulomb failure criterion. The microscopic parameters in this contact law involve elastic parameters (E,K_T/K_N,β_r) as well as rupture parameters ($\emptyset_{micro}$ and η_r). E_i is the particle modulus; K_N and K_T are the normal and tangential stiffness at the contact point; β_r is the rolling resistance coefficient; $\emptyset_{micro}$ is the microscopic friction angle between particles, and η_r is a dimensionless coefficient to define a threshold for the resistant moment. To keep the paper size manageable, the details of the contact model and its fundamental equations are omitted in this manuscript.

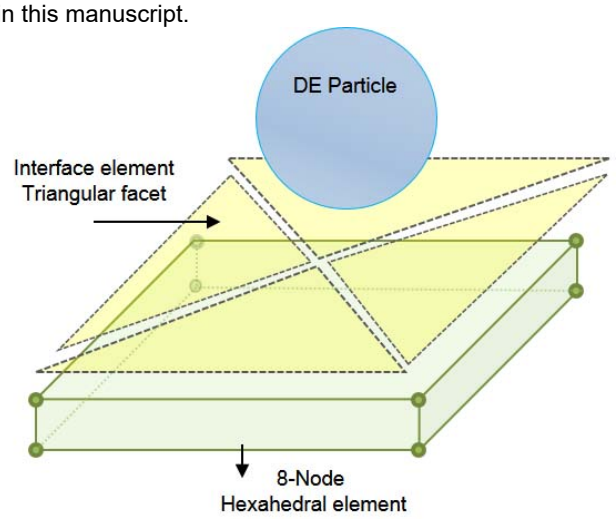

Figure 2. Coupling FE and DE using interface elements

3.3 Interface elements

Triangular shaped facets are used as interface elements in the coupled model to connect the FE and DE domains. These elements are generated directly following the finite element nodes. As hexahedral elements are used for the FE domain, the contact surface between the FE and DE domains is divided into four interface elements by adding a temporary node defined as follows:

$$X^{(O)} = \frac{1}{4}\sum_{i=1}^{4} X^{(i)} \quad (4)$$

where $X^{(i)}$ is the coordinate of node i of the quadrilateral. Fig. 2 shows a schematic of the interaction between a finite element, interface elements, and a DE particle. The contact law between the interface elements and DE particles is the same as particle-particle interaction mentioned in the previous section. After the creation of a particle-interface contact, the normal penetration and incremental tangential displacement of the contact are calculated. The normal and tangential interaction forces are calculated based on these two values. Eq. 5 is used to compute the transmitted forces to the FE nodes using interaction forces.

$$\vec{F}_i = \vec{F}_{contact} \cdot N_i \quad (5)$$

where $\vec{F}_{contact}$ is the total contact force determined by adding the normal and the tangential force vectors ($\vec{F}_N + \vec{F}_T$), and N_i is the shape function calculated using the natural coordinates of the contact point.

After deformation of the FE domain and movement of DE particles as a result of the contact forces ($\vec{F}_{contact}$), new location of the interface elements are computed. Based on these changes, new interface-particle interactions are generated. A typical FE-DE computational cycle and its main steps were explained in detail by Dang and Meguid (2010a, 2013).

4 MODEL GENERATION

The numerical model is created based on the experiments discussed in section 2. The foundation and drainage layers are modeled using spherical particles. To create these layers, two clouds of non-contacting particles are generated following the particle size distribution presented in Fig. 1. Then, for subgrade soil, the radius expansion method is employed to reach the target porosity and density. Since it is numerically impossible to model the exact size of the sand particles, particle up-scaling is required. Considering the minimum L/d (Smallest length of the model / median diameter of the simulated particles) ratio of 20 based on the recommendations of Schopfer et al. (2007) and Ding et al. (2014), Scale factor of 17 is chosen for this layer and a total of over 120,000 particles are generated.

For the drainage layer, the generated particles are allowed to move under gravity without any compaction following the same procedure of the experiments. Using scale factor of 1, a total of 1,350 gravel particles are generated with a final thickness of 300 mm. 3D and 2D views of the generated sample are shown in Fig. 3.

The GM is modeled using 8-noded hexahedral elements. A linear elastic material model is used following the properties listed in Table 1. The GM sheet is square shaped (590 x 590) with a thickness of 1.5 mm. A total of 900 finite elements and 7200 interface elements are used in this study. The artificial wrinkle is shaped in the model based on the height and width used in the experiments. The geometry of the wrinkled GM sheet is presented in Fig. 4.

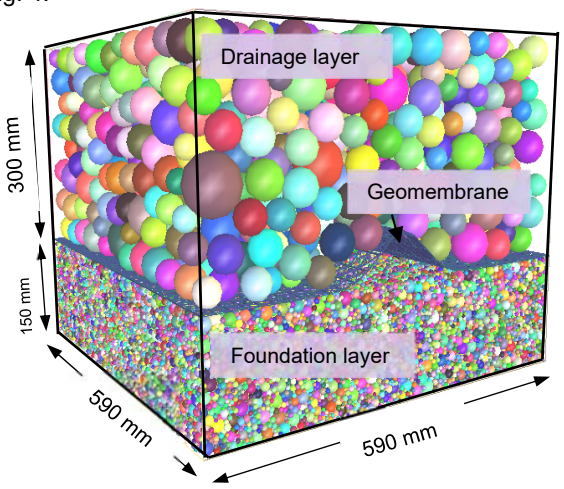

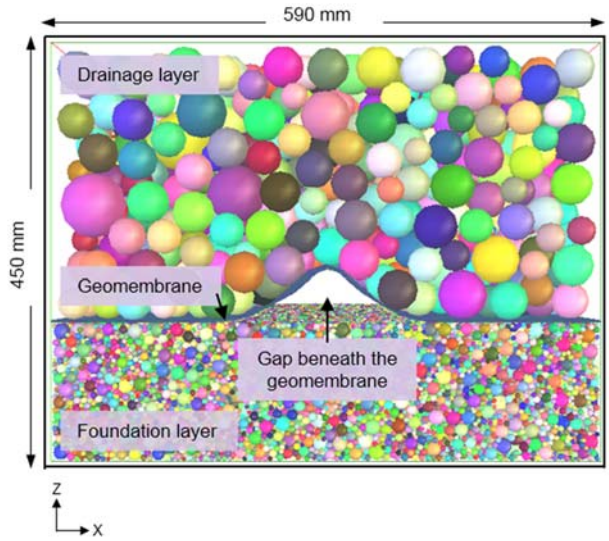

Figure 3. Initial coupled FE-DE specimen

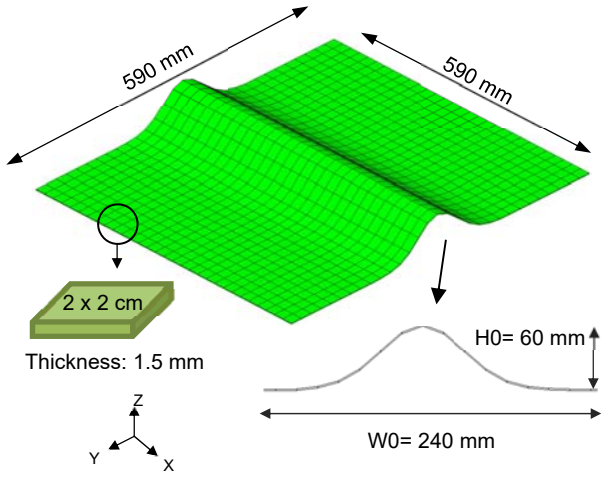

Figure 4. Geometry of the simulated geomembrane sheet

To determine the input parameters of the spherical particles in the DE simulation, model calibration is needed. This requires triaxial and direct shear test results of the drainage and subgrade layers. As these results are not available, reasonable material parameters are assumed based on previous studies conducted by McGill Geogroup (eg. Tran et al. 2013, Meidani et al. 2017). Table 2 shows the input parameters used in DE simulation. To evaluate the effect of different parameters on the response of the wrinkle, a series of twelve different numerical models are analyzed and the results as well as the input parameters are summarized in Table 3. Simulation 1 is the reference test (test 1) and the highlighted values represent the range of examined parameters.). Hence, tests 2 and 3 focus on the change in subgrade friction angle and tests 4 and 5 evaluate the effect of subgrade Young's modulus. The effect of drainage layer friction angle is investigated in tests 6 and 7; tests 8 and 9 consider a change in the Young's modulus of the drainage layer. Finally, tests 10, 11 and 12 are conducted to assess the effect of overburden pressure on the response of the wrinkle.

Table 2 Input parameters of the simulation

Discrete particles	Value
Density of gravel particles (kg/m^3)	2750
Density of sand particles (kg/m^3)	2600
Gravel particle modulus *E* (MPa)	200
Sand particle modulus *E* (MPa)	150
Ratio K_T/K_N	0.3
Micro friction angle of gravel particles	36°
Micro friction angle of sand particles	30°
η_r	1.0
Rolling resistance coefficient (β_r)	0.3
Damping coefficient	0.2
Finite elements (GM)	**Value**
Young's modulus *E* (MPa)	300
Poisson's ratio *v*	0.3
Interface elements	**Value**
Material modulus *E* (MPa)	175
Ratio K_T/K_N	0.3
Micro friction angle ($\emptyset_{micro}$)	30°

Table 3. Summary of tests configurations

Test	Test conditions				
	Foundation layer		Drainage layer		
	E (Pa)	φ °	*E* (Pa)	φ °	
1	1.50E+08	30	2.00E+08	36	250
2	1.50E+08	25	2.00E+08	36	250
3	1.50E+08	20	2.00E+08	36	250
4	2.00E+08	30	2.00E+08	36	250
5	1.00E+08	30	2.00E+08	36	250
6	1.50E+08	30	2.00E+08	40	250
7	1.50E+08	30	2.00E+08	45	250
8	1.50E+08	30	2.50E+08	36	250
9	1.50E+08	30	1.50E+08	36	250
10	1.50E+08	30	2.00E+08	36	500
11	1.50E+08	30	2.00E+08	36	750
12	1.50E+08	30	2.00E+08	36	1050

5 RESULTS AND DISCUSSION

The result of the reference test (Test 1) is presented first in this section. Fig. 5 shows the initial and deformed shape of the GM in test 1 under vertical pressure of 250

kPa. It can be seen that both the wrinkle height and width decreased by 39% and 31% after applying the vertical pressure and the gap became smaller, however, it did not completely disappear. Fig. 6 shows the 2D view of the model used in Test 1 after applying the load. The reduction of the gap size is related to the vertical movement of the drainage layer and the GM sheet, however, due to the stiffness of the foundation layer, no significant upward vertical movement developed in sand. This finding is in agreement with that reported by Brachman and Gudina (2008) who concluded that the physical gap was reduced but remained when the GM was underlain by a firm sand foundation. A summary of the calculated test results with the percentage change in wrinkle height and width are presented in Table 4.

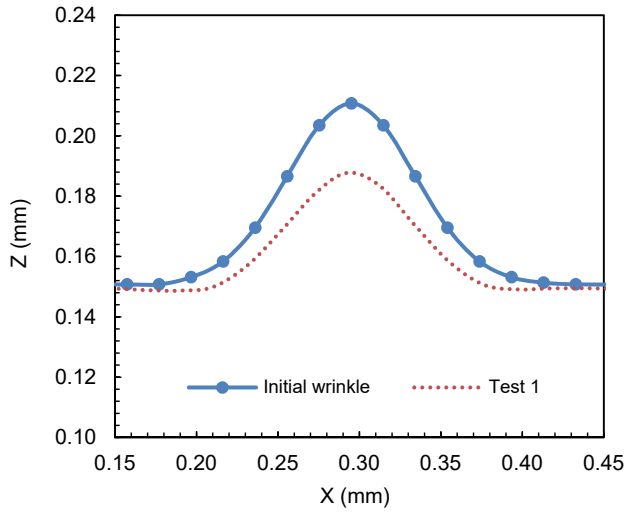

Figure 5. Initial and final shapes of the geomembrane wrinkle subjected to 250 KPa

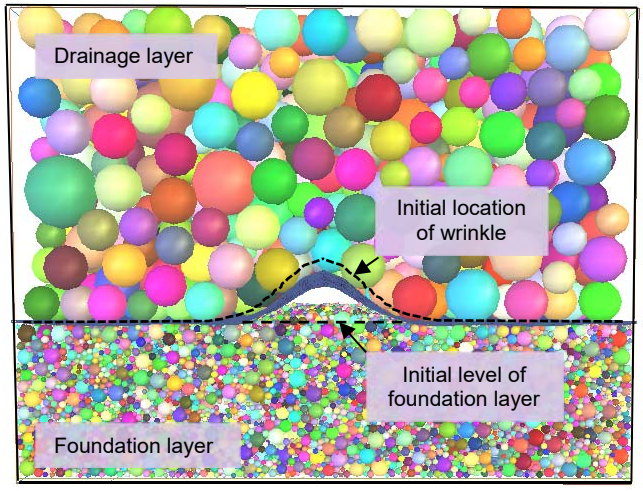

Figure 6. 2D view of the model after applying the vertical load in Test 1, initial and final location of the GM wrinkle is illustrated.

Tests 2 and 3 are performed to study the effect of the friction angle of the sand layer on the wrinkle deformation. Fig. 7 shows that by decreasing the friction between sand particles, wrinkle deformation increased and the gap gets smaller. It can be seen from Table 4 that by changing the friction angle from 30° in test 1 to 20° in test 3, the wrinkle height and width decreased by 8 and 21 mm. This response of the GM could be related to the relative movement of sand particles at lower friction angle under vertical load, which allows GM to deform easier.

Table 4. Summary of the tests results. Wrinkle initial height and width are H_0=60 mm and w_0=240 mm

Test	Final wrinkle geometry					
1	36.7	23.3	39	166	74	31
2	32.3	27.7	46	156	84	35
3	28.1	31.9	53	145	95	40
4	39.6	20.4	34	169	71	30
5	32.5	27.5	46	161	79	33
6	38.2	21.8	36	168	72	30
7	39.2	20.8	35	173	67	28
8	40.7	19.3	32	180	60	25
9	31.0	29.0	48	149	91	38
10	31.9	28.1	47	153	87	36
11	28.8	31.2	52	146	94	39
12	26.2	33.8	56	140	100	42

The effect of Young's modulus of the subgrade layer on the wrinkle deformation is evaluated in tests 4 and 5 and the results are presented in Fig. 8. By decreasing Young's modulus of the sand layer, the wrinkle deformation increased. Based on the data presented in Table 4, the change in wrinkle height is more significant in comparison with wrinkle width. This response of the wrinkle can be attributed to the higher settlement of the softer foundation under vertical load.

Tests 6 and 7 are performed to evaluate the effect of the friction angle of the drainage layer on the wrinkle deformation. Results of these two simulations with respect to the reference test are presented in Fig. 9. It is found that the friction angle of the gravel particles doesn't have a significant effect on the response of the GM and the gap size is similar in all three tests.

Two additional tests are developed to investigate the response of geomembrane wrinkle to the change in Young's modulus of the drainage layer. Fig. 10 shows the results of Tests 8 and 9 and the reference test. It is concluded that by decreasing the gravel particles Young's modulus, the wrinkle deformation increased and the gap size became smaller. Detailed results of these two tests are presented in Table 4. It can be seen that increasing the E value by 40%, the wrinkle height and width decreased 16% and 13%, respectively.

The response of the GM wrinkle to the vertical pressure are evaluated by performing three Tests (Tests 10, 11 and 12) and the results are plotted in Fig. 11 and presented in Table 4. Data shows that the vertical

pressure and wrinkle deformation are proportional and at higher applied load, a smaller gap is expected. It is interesting to note that even at applied pressure of up to 1,100 kPa the gap was reduced but still remained. This is consistent with the observations of Gudina and Brachman (2006). In addition, the vertical displacement of the geomembrane in test 12 is plotted in Fig. 12. It can be seen that most of the vertical movement occurred at the crown of the wrinkle. Displacement in the flat areas of the GM sheet could be related to the indentation made by the course gravel backfill above the GM.

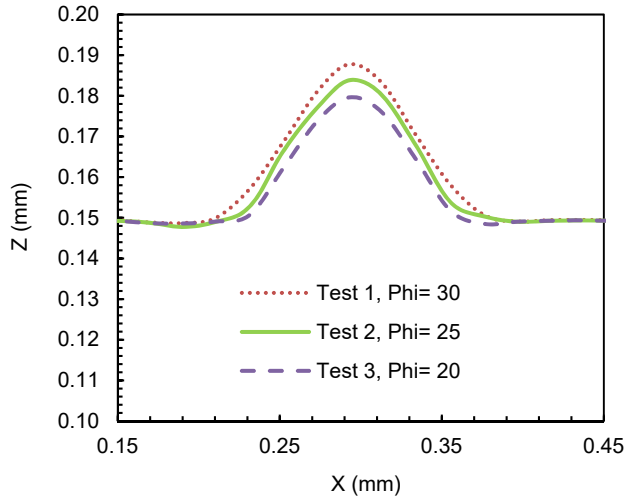

Figure 7. Dependency of wrinkle deformation to foundation layer friction angle

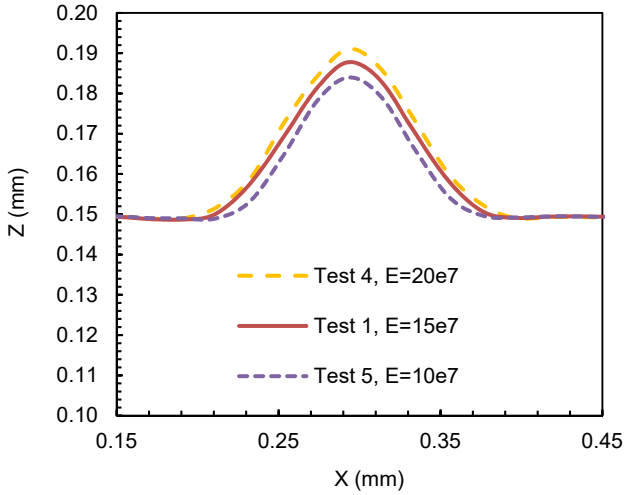

Figure 8. Dependency of wrinkle deformation to foundation layer Young's modulus

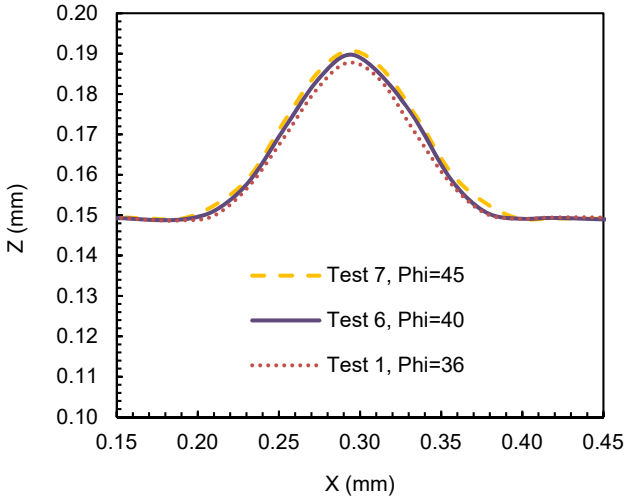

Figure 9. Dependency of wrinkle deformation to drainage layer friction angle

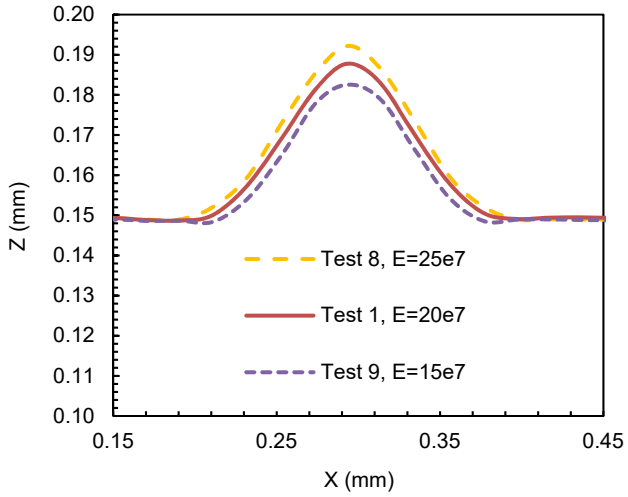

Figure 10. Dependency of wrinkle deformation to drainage layer Young's modulus

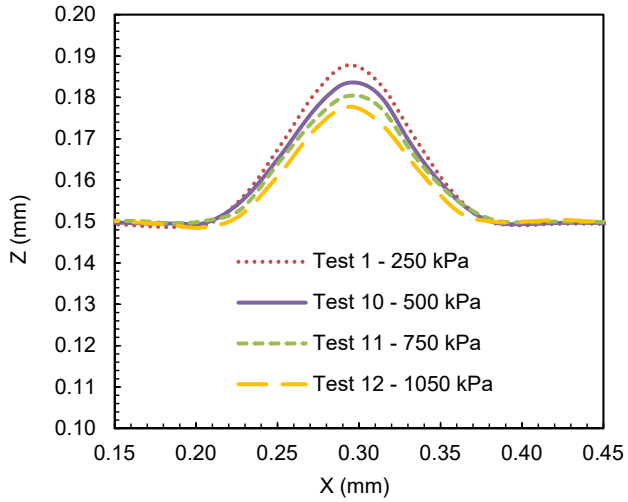

Figure 11. Dependency of wrinkle deformation to vertical pressure

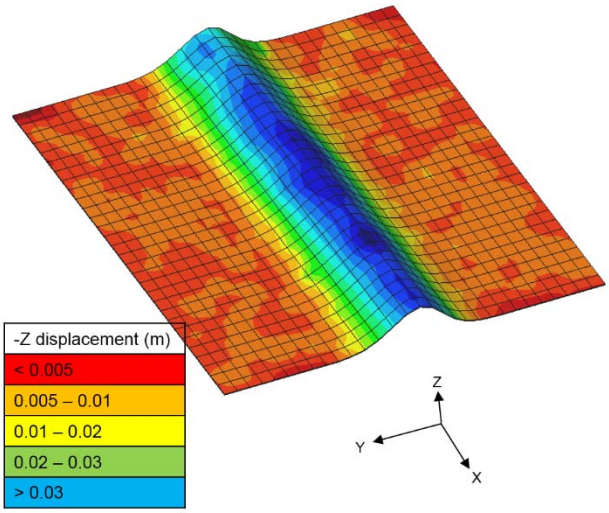

Figure 12. Geomembrane wrinkle vertical displacement at vertical pressure 1,100 kPa

6 CONCLUSION

This study has investigated the response of GM wrinkle using coupled finite-discrete element framework. The geomembrane is placed between compacted sand foundation and gravely drainage layer. Effect of different parameters such as sand and gravel friction angle and Young's modulus and the applied vertical pressure on the wrinkle deformation are investigated. The main conclusions are:

1- The wrinkle moved downwards and inwards (toward the center) in all tests under vertical pressure. Hence, the gap size get smaller but the gap remains under the geomembrane.
2- Increasing the sand layer friction angle and Young's modulus decreases the wrinkle deformation.
3- Changing the drainage layer friction angle doesn't have a significant effect on wrinkle shape, but increasing the Young's modulus affects the height and width of the wrinkle with bigger gap remains beneath the geomembrane.
4- The wrinkle height and width decreases when subjected to vertical pressure. Increasing the pressure makes the gap between the GM and the foundation smaller, but remained as the firm sand foundation layer doesn't fill in the gap.

It should be noted that the reported values for wrinkle height and width are based on numerical simulations using coupled model that has not been properly calibrated. However, the parametric study illustrated the pattern of the wrinkle deformation under different conditions. Finally, the finite-discrete element framework has proven to be efficient in capturing the response of the GM and the surrounding soils.

7 ACKNOWLEDGMENT

This research is supported by the Natural Sciences and Engineering Research Council of Canada (NSERC). Financial support provided by McGill Engineering Doctoral Award (MEDA) to the first author is appreciated.

8 REFERENCES

Brachman, R. W. I., & Gudina, S. (2008). Geomembrane strains from coarse gravel and wrinkles in a GM/GCL composite liner. Geotextiles and Geomembranes, 26, 6, 488-497.

Dang, H.K., Meguid, M.A., (2010a). Algorithm to generate a discrete element specimen with predefined properties. International Journal of Geomechanics 10 (2), 85-91.

Dang, H.K., Meguid, M.A., (2013). An efficient finite-discrete element method for quasi-static nonlinear soil-structure interaction problems. International Journal for Numerical and Analytical Methods in Geomechanics 37 (2), 130-149.

Ding, X., Zhang, L., Zhu, H., & Zhang, Q., (2014). Effect of Model Scale and Particle Size Distribution on PFC3D Simulation Results. Rock Mechanics and Rock Engineering. 47, 2139-2156.

Gudina, S., & Brachman, R. W. I. (2006). Physical Response of Geomembrane Wrinkles Overlying Compacted Clay. Journal of Geotechnical and Geoenvironmental Engineering, 132, 10, 1346-1353.

Meidani, M., Meguid, M. A., & Chouinard, L. E., (2017). Evaluation of Soil–Pipe Interaction under Relative Axial Ground Movement. Journal of Pipeline Systems Engineering and Practice, 4, 4017009.

Pelte, T., Pierson, P., and Gourc, J. P. (1994). Thermal analysis of geomembrane exposed to solar radiation. Geosynthet. Int., 1(1), 21–44.

Rowe, R. K., Quigley, R. M., Brachman, R. W. I., Booker, J. R. (2004). Barrier systems for waste disposal facilities, E&FN Spon, London.

Schöpfer, MPJ., Childs, C., Walsh, JJ., 2007. Two-dimensional distinct element modeling of the structure and growth of normal faults in multilayer sequences: 1. Model calibration, boundary conditions, and selected results. Journal of Geophysics Res 112(B10):B10401. doi:10.1029/2006jb004902.

Soong, T.-Y., and Koerner, R. M. (1998). Laboratory study of high density polyethylene waves. Proc., 6th Int. Conf. on Industrial Fabrics Association International, Geosynthetics, St. Paul, Minn., 301–306.

Tran, V. D. H., Meguid, M. A., and Chouinard, L. E. (2013). "A finite-discrete element framework for the 3D modeling of geogrid-soil interaction under pullout loading conditions." Geotext. Geomembr., 37(1-9).